Shear-induced alignment and dynamics of elongated granular particles

Tamás Börzsönyi,[1,*] Balázs Szabó,[1] Sandra Wegner,[2] Kirsten Harth,[2] János Török,[3] Ellák Somfai,[4] Tomasz Bien,[2] and Ralf Stannarius[2]

[1]*Institute for Solid State Physics and Optics, Wigner Research Center for Physics, Hungarian Academy of Sciences, P.O. Box 49, H-1525 Budapest, Hungary*
[2]*Otto-von-Guericke-University, D-39106 Magdeburg, Germany*
[3]*Institute of Physics, Budapest University of Technology and Economics, H-1111 Budapest, Hungary*
[4]*Department of Physics and Centre for Complexity Science, University of Warwick, Coventry CV4 7AL, United Kingdom*

The alignment, ordering, and rotation of elongated granular particles was studied in shear flow. The time evolution of the orientation of a large number of particles was monitored in laboratory experiments by particle tracking using optical imaging and x-ray computed tomography. The experiments were complemented by discrete element simulations. The particles develop an orientational order. In the steady state the time- and ensemble-averaged direction of the main axis of the particles encloses a small angle with the streamlines. This shear alignment angle is independent of the applied shear rate, and it decreases with increasing grain aspect ratio. At the grain level the steady state is characterized by a net rotation of the particles, as dictated by the shear flow. The distribution of particle rotational velocities was measured both in the steady state and also during the initial transients. The average rotation speed of particles with their long axis perpendicular to the shear alignment angle is larger, while shear aligned particles rotate slower. The ratio of this fast/slow rotation increases with particle aspect ratio. During the initial transient starting from an unaligned initial condition, particles having an orientation just beyond the shear alignment angle rotate opposite to the direction dictated by the shear flow.

I. INTRODUCTION

Granular flows involving elongated particles are very important in agriculture, industry, and natural processes. In a shear flow the interparticle contact forces often lead to orientational ordering and alignment of the particles. While the basic properties of granular flows have been widely studied for rapid (collisional), quasistatic, and intermediate regimes [1–24], the flow properties of samples consisting of elongated objects is not well understood. After early experiments on grass seeds [6] and rice grains [7], recent numerical studies focused on shear flows of ellipsoidal particles [9,19,20]. These latter studies revealed the topology of the contact forces [19,20] for sheared ellipsoidal particles and also described how the stresses and the corresponding particle orientations depend on the aspect ratio of the ellipsoids [9]. In a recent work [25] we have demonstrated the basic properties of the shear induced order focusing on the time- and ensemble-averaged properties only. We compared these to various systems including colloids, nanoparticles, and nematic liquid crystals. We have also shown that the shear alignment results in a considerable reduction of the effective friction of the material.

In the present paper we explore the behavior of individual particles: we detect their rotation induced by the shear flow, and measure the average rotation speed as a function of particle orientation during stationary shear and also during the transient when shear is applied to an initially unoriented or misoriented system. We also present the basic properties of the shear aligned state for an extended set of materials. Details of our experimental and numerical methods are given as well.

II. EXPERIMENTAL SETUP

A. Experimental geometry and materials

The granular material was placed in a so-called cylindrical split bottom cell (see Fig. 1). In this geometry a circular plate at the bottom of the container is rotated with a constant speed. If the granular layer is thin enough (compared to the size of the rotating plate) the middle part of the granular sample will rotate with the plate like a rigid body. The outer part of the sample (near the walls of the cylindrical container) remains stationary. The region in between these undisturbed parts is continuously sheared and is called the shear zone (or shear band). The shear zone is indicated with dark gray in Fig. 1(a). Other properties of this configuration, like the precise geometry of the shear zone and its dependence on the filling height were described in previous studies [21,22,26].

In our experiments, various prolate particles were investigated as shown in Fig. 1(d). The length to diameter (or aspect) ratios of the particles were $L/d = 2.0$, 3.4 and 4.5 (rice grains), 1.4 and 3.5 (glass cylinders), and 2.0, 3.3, 5.0 (wooden pegs). Two experimental methods were used to visualize and characterize the shear-induced alignment: (i) complete three-dimensional (3D) imaging of the sample with x-ray computed tomography (CT) and (ii) optical imaging of the particles at the upper surface of the system with a digital camera. Pegs were investigated by x-ray CT, glass cylinders and rice particles by optical imaging. The diameter of the rotating plate was $D_p \approx 80\,d$, while the container diameter was $D_c \approx 140\,d$ in both experiments. We used a typical filling height of $H \approx 11d \approx 0.14\,D_p$.

B. Particle detection by x-ray computed tomography

The complete 3D arrangement of all particles in the shear zone was determined experimentally for three samples (pegs
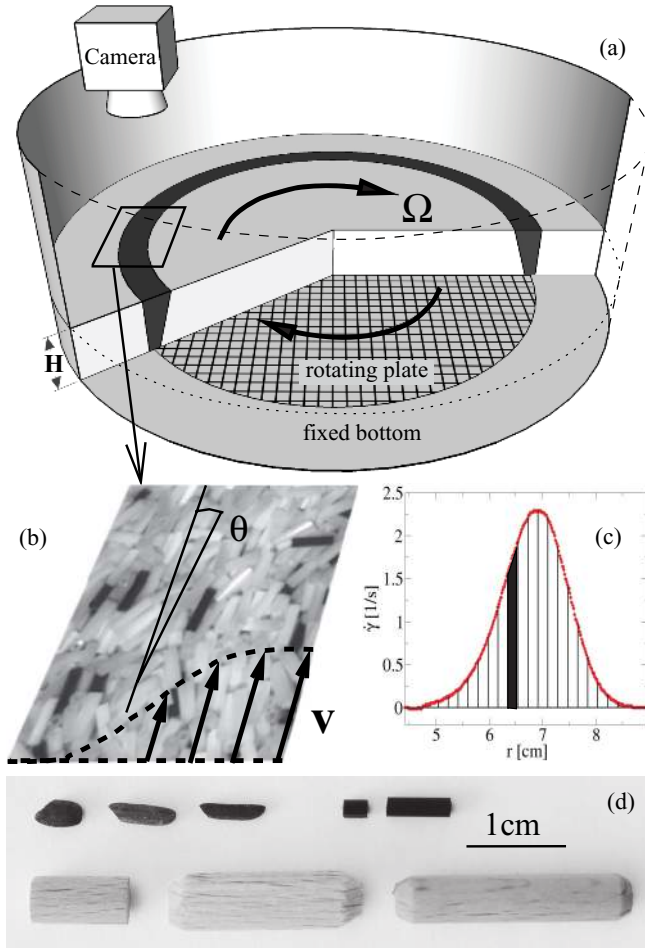
*borzsonyi.tamas@wigner.mta.hu

FIG. 1. (Color online) (a) Illustration of the experimental setup. The granular material consisting of elongated grains is sheared as the circular bottom plate continuously rotates. Shear strain is localized in the region marked with dark gray. (b) Example image of the surface of the shear zone for glass cylinders with $d = 1.9$ mm and $L/d = 3.5$. The typical orientation of the particles encloses a small angle θ with respect to the streamlines (i.e., the particles are slightly inclined towards the velocity gradient). (c) Shear rate $\dot{\gamma}$ as a function of the radius r; also glass cylinders, $L/d = 3.5$. Bins with different average shear rate are marked. (d) Photographs of the particles studied, with $L/d = 2.0, 3.4, 4.5$ (rice), as well as 1.4 and 3.5 (glass cylinders), and 2.0, 3.3, 5.0 (pegs).

with $L/d = 2.0, 3.3$ and 5.0) using x-ray CT [27]. For these measurements we used a medical angiography system (i.e., a rotational c-arm-based x-ray device equipped with a flat-panel detector).[1] The spatial resolution of the device was between 1.5 pixel/mm and 2 pixel/mm. The primary purpose of these experiments was to show that the order and alignment data extracted from surface particles are representative for the global order in the shear zone, with only slight variations. The particles were detected by applying a watershed algorithm to the recorded images. The particles' orientation was defined as the direction of the largest eigenvector of the individual

moment of inertia tensors. The shear-induced orientational order is monitored by diagonalizing the symmetric traceless order tensor $\boldsymbol{T}$

$$T_{ij} = \frac{3}{2N} \sum_{n=1}^{N} \left[\ell_i^{(n)} \ell_j^{(n)} - \frac{1}{3} \delta_{ij} \right], \tag{1}$$

where $\vec{\ell}^{(n)}$ is a unit vector along the long axis of particle n, and the sum is over all N detected particles. The largest eigenvalue of $\boldsymbol{T}$ is the primary order parameter S. The shear-induced alignment is characterized by the average alignment angle θ_{av}, which is the angle of the corresponding principal axis of $\boldsymbol{T}$ measured with respect to the flow direction [see Fig. 1(b)]. Positive θ corresponds to inclination towards the velocity gradient. The components of $\boldsymbol{T}$ were determined both near the surface (particles with centers in the top ≈ 1 cm layer, approximately 2 particle diameters) and in the bulk (2 cm thick layer below), corresponding to about 10000 and 20000 particle positions, respectively. The experiment is described in detail in Ref. [27].

C. Optical particle detection

For rice grains and glass cylinders, the top surface of the whole sample was monitored with a digital camera using a frame rate of 18 fps. As an illustration, a section of an image is shown in Fig. 1(b). The shear rate $\dot{\gamma}$ is not constant across the shear zone, but it changes with the radius r measured from the center of the cell. It is expressed as $\dot{\gamma} = \mathrm{d}v(r)/\mathrm{d}r - v(r)/r$, where $v(r)$ is the tangential velocity of the material. The tangential velocity $v(r)$ was determined using a self-developed particle image velocimetry (PIV) code and the time-averaged shear rate was calculated. This shear rate profile is presented in Fig. 1(c). The shear zone was divided into about 20 bands (widths 0.19 cm $\approx d$) as illustrated in Fig. 1(c). The average shear rate was determined for each band. The orientation and in-plane length of colored tracer grains (6% of the sample) were detected, yielding about 60000 particle positions in each band for each type of grain. This way, a single experiment with constant rotation speed Ω provides information about the shear rate dependence of the alignment [23]. In order to cover a wide range of shear rates, the experiments were repeated at three different values of Ω.

D. Torque measurement

In order to monitor changes in the mechanical resistance of the sample against shearing, we continuously measured the torque needed to maintain a constant rotation rate of the bottom plate during the evolution of the alignment. This has been done the following way. The driving motor was mounted on a rotating table. To keep the body of the motor fixed and let the plate rotate in the sample container, we use a load cell attached to the body of the motor. We measure the torque needed to hold the motor while the granular material is sheared with a constant speed by the rotating bottom plate.

III. NUMERICAL SETUP

Discrete element method (DEM) simulations were performed to complement the experiments. A modified
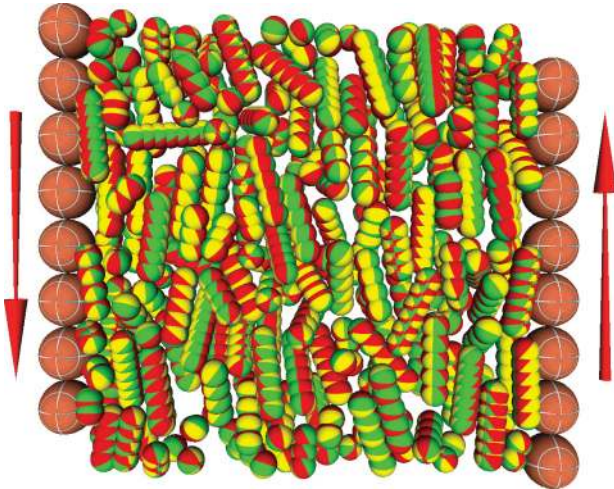
FIG. 2. (Color online) Example cut of the numerical setup. The wall consisting of larger spheres imposes constant pressure and stationary shear to the sample. The snapshot was taken in the steady state, where most of the particles are shear aligned.
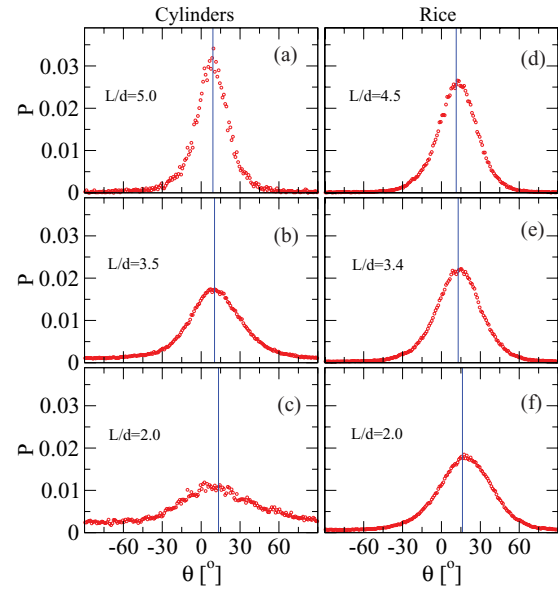

FIG. 3. (Color online) Distributions of the orientational angle θ of the particles with respect to the streamlines for (a)–(c) cylinders with $L/d = 5.0$, 3.5, and 2.0, and (d)–(f) rice particles with $L/d = 4.5$, 3.4, and 2.0, respectively. For panels (a) and (c) data obtained by x-ray CT, other data obtained by optical particle detection. The vertical blue line corresponds to the stationary average orientation, Θ_{av}.

version [24] of the general purpose molecular dynamics code LAMMPS [28] was used to generate stiff elongated particles by gluing spheres together. Long particles generated this way have parts with concave curvature and thus are prone to interlock if their structure is identical. Therefore we prepared polydisperse samples by allowing the variation of the following quantities: the radius of the spheres by 10%, the length of the particles by 10%, and the overlap of the spheres between 30–70% of the radius. We also varied the number of spheres required to build up a long particle.

The dynamics of 700–1200 elongated particles was modeled in simple Couette flow, where the parallel walls were moved in the opposite directions as indicated in Fig. 2 by the arrows. The walls consisted of twice as large spheres as the average particle diameters. In the other two directions periodic boundary conditions were chosen. The particles were confined with constant pressure during shear. The generated shear rate was relatively uniform across the sample [29].

IV. RESULTS

A. Stationary state

As described in Sec. II, a sufficiently large set of particle positions and corresponding orientations were detected using either optical imaging at the surface or x-ray CT in the whole sample. The distribution of the alignment angles θ (measured in the shear plane with respect to the local direction of the streamlines) is presented for cylinders with length to diameter ratios of $L/d = 5.0$, 3.5, and 2.0 and and rice with $L/d = 4.5$, 3.4, and 2.0 in Figs. 3(a)–3(c) and Figs. 3(d)–3(f), respectively. The first thing to note is the aspect ratio dependence of the distributions. The graphs show that increasing L/d leads to a narrower distribution (i.e., a higher degree of shear-induced ordering). The time- and ensemble-averaged particle orientation Θ_{av} was determined by fitting the data by a Gaussian (with the constant offset subtracted), and is illustrated with a vertical (blue/gray) line in Figs. 3(a)–3(f). Thus, asymptotically the average orientation encloses a small angle Θ_{av} with the

streamlines, as it is illustrated in Fig. 1(b) for $L/d = 3.5$. The second interesting observation is that for cylinders ($L/d = 3.5$ and 2.0) the distribution is broader than for ellipses with similar aspect ratio. This can be understood by analyzing the shortest sample ($L/d = 1.4$) in Fig. 4. Here, the distribution has two peaks, see the zoomed inset of Fig. 4(a). This suggests that these grains align with their longest extension (diagonal) in the preferential direction. Since we determine the particle orientation by measuring the orientation of the symmetry axis, the distribution of the detected angles has two peaks, approximately $2 \arctan(1/1.4) = 71°$ apart, which correspond to the two-particle configurations illustrated in Fig. 4(b) for $L/d = 1.4$. The effective average alignment angle in this case is between the angles corresponding to the two peaks (i.e., around $\Theta_{av} = 29°$). Getting back to the case of longer cylinders, the above described effect could be one of the factors leading to a widening of the distributions (especially for the case of cylinders with sharp edges) compared to the case of rice with similar aspect ratio [compare Figs. 3(c) and 3(f)].

Figure 3 also illustrates the typical scatter of the angular distributions obtained by the two methods (optical or x-ray measurements). Data for all rice samples as well as for cylinders with $L/d = 3.5$ were obtained by optical detection and the histograms presented were created using about 200 000 data points, while the data for pegs with $L/d = 5.0$ and 2.0 were collected from the surface region of the whole shear zone by x-ray CT (about 10 000 data points). Due to the smaller number of data points, the scatter of the distributions is larger in these latter cases.

As explained before, the center Θ_{av} of the orientational distribution was determined by fitting a Gaussian, and the order parameter S, defined as the largest eigenvalue of $\boldsymbol{T}$, was calculated. Note that S is related to the width of
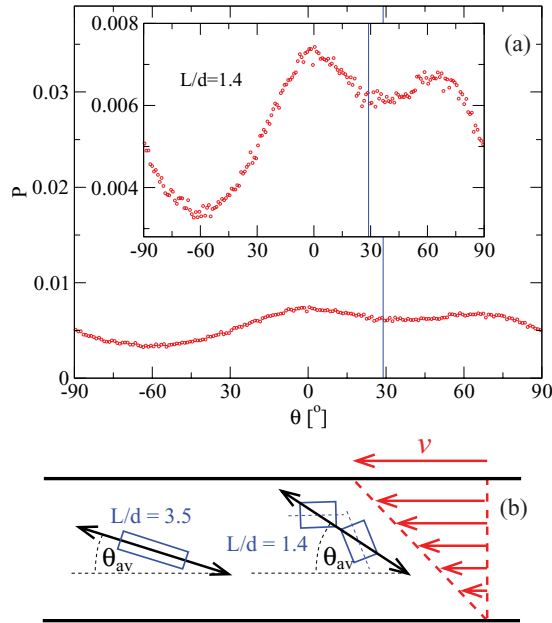
FIG. 4. (Color online) (a) Distribution of the orientational angle θ of the particles with respect to the streamlines for cylinders with $L/d = 1.4$. Data obtained by optical particle detection. The inset in (d) is the same data on a different scale. The vertical blue line corresponds to the average orientation, Θ_{av}. (b) Illustration of typical (average) particle alignment for longer ($L/d = 3.5$) and shorter $L/d = 1.4$ cylinders.

the angular distribution σ. As seen in Fig. 5, Θ_{av} and S (as well as σ, not displayed) are practically shear rate independent across more than three decades of $\dot{\gamma}$. The slight decrease of S observed for two samples of rice [25] is not observed here for cylinders. The data points were collected using three different rotation rates ($\Omega = 0.26$, 0.52, and 4.2 rad/s) of the bottom plate. The spatial variation of $\dot{\gamma}$ in the shear zone allows to span a relatively wide range of $\dot{\gamma}$ for each rotation rate, as marked in Fig. 5(b). In terms of inertial number (defined as $I = \dot{\gamma} d \sqrt{\rho/P}$, where ρ is the density of particles and for the hydrostatic pressure P we use an indicative value taken at depth d), our measurements span the range between 0.0002 to 0.4.

The fact that the average orientation of the particles in the aligned state is shear rate independent is similar to the well-studied *flow alignment* of nematic liquid crystals. We have quantitatively compared our observations to the properties of nematics in Ref. [25], here we only wish to stress that the strong similarities with nematics indicate that the shear alignment is robust and is of geometrical origin. Namely, even if the aspect ratios of the building blocks (molecules and granulates) are similar, there are other important differences between the two systems (e.g., thermal fluctuations are important for molecules while they are negligible in the granular case). Also, the interparticle forces have very different character: the molecules experience attractive forces (dipole-dipole, van der Waals), while the granular particles investigated here interact only via hardcore repulsion and friction.

As seen in Fig. 5, the average alignment angle Θ_{av} depends only on the properties of the particles. The shear-rate-independent Θ_{av} has been determined for all eight samples
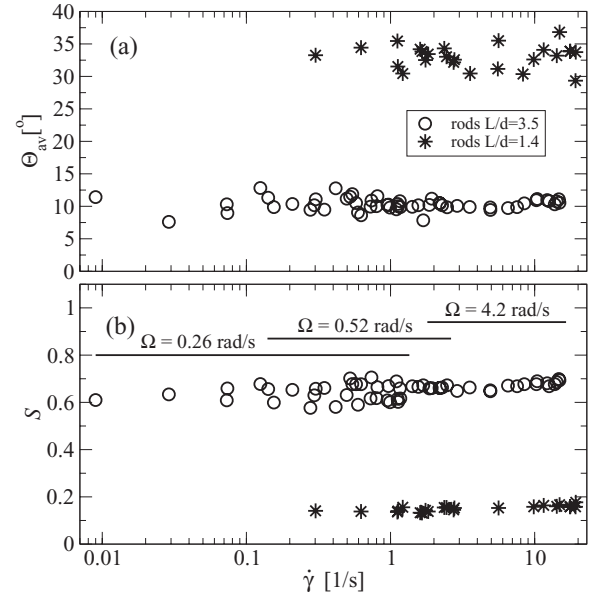

FIG. 5. (a) The average orientational angle Θ_{av} of the particles with respect to the streamlines and (b) the order parameter S as a function of the shear rate $\dot{\gamma}$. Data obtained by optical measurements for glass cylinders with length to width ratios $L/d = 1.4$ and 3.5. Both, Θ_{av} and S are independent of the shear rate.

and it is presented as a function of the aspect ratio L/d in Fig. 6. The plot combines the bulk and surface data from x-ray tomography, the surface data from optical experiments, and the numerical results in bulk plane Couette flow. We find a systematic decrease of Θ_{av} with increasing length to width ratio for a given shape family (rice or cylinders). Results of the numerical simulations nicely agree with the experimental data. At comparable aspect ratios, the alignment angle appears to be systematically smaller for cylinders than for ellipsoids.

Focusing on the dynamics of individual grains during stationary shear, the orientation of the majority of the particles
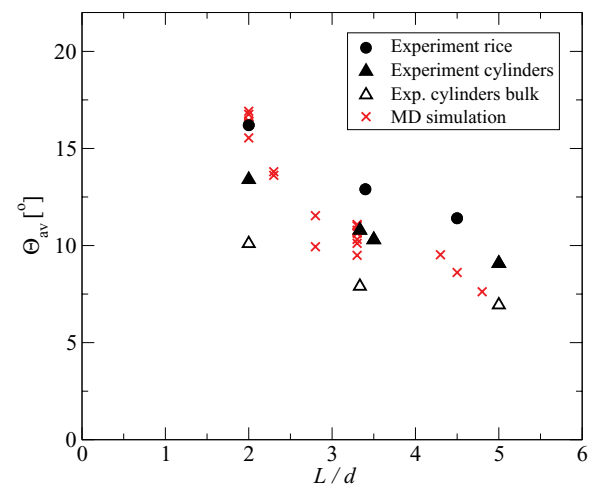

FIG. 6. (Color online) The average orientational angle Θ_{av} as a function of the length to diameter ratio L/d of the particles obtained by experiments ($\bullet$, $\blacktriangle$, $\triangle$) and numerical simulations ($\times$).
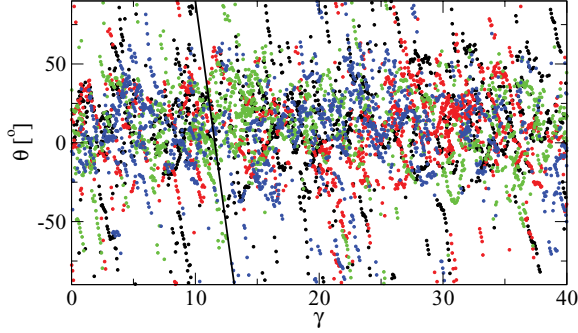
FIG. 7. (Color online) Evolution of the particle orientations θ as a function of strain γ in the stationary state for glass cylinders with $L/d = 3.5$. Data obtained by optical particle detection. The black line corresponds to $d\theta/d\gamma = -1$ (in radians). For better visualization of the trajectories we used four different colors.

stays within a range of $\Theta_{av} - \sigma < \theta < \Theta_{av} + \sigma$, where σ is the standard deviation of the Gaussian fit of the orientational distributions. This range is seen as a dense band in Fig. 7 between the angles of $-20°$ and $35°$ for the case of glass cylinders with $L/d = 3.5$. In this range the particles rotate forward or backward with essentially equal probability. Outside this range the particles are rarely seen and they rotate relatively quickly forward as it is indicated by the steep trajectories in Fig. 7. For these measurements data have been taken from the center of the shear zone, where the shear rate $\dot{\gamma}$ is nearly constant.

The distribution of the particle rotation velocity $\omega = d\theta/dt$ has been determined as a function of θ and the resulting plot is shown in Fig. 8. Here ω is normalized by the average shear rate at the location of the particle. As it is seen $\omega/\dot{\gamma}$ is better defined for the above mentioned range ($\Theta_{av} - \sigma < \theta < \Theta_{av} + \sigma$) near Θ_{av}, while the distribution is wider (i.e. ω is less well defined) near $\theta = \Theta_{av} + \pi/2$. At $\theta = \Theta_{av} + \pi/2$ we find an average rotation speed $\omega/\dot{\gamma} \approx -1$ rad/unit strain. Thus, at this angle the rotation speed of the particles is maximal, it reaches the value corresponding to the local vorticity of the shear flow.

We calculated the averages of the rotation velocity distributions normalized by the shear rate, $\omega_{av}/\dot{\gamma}$, for various
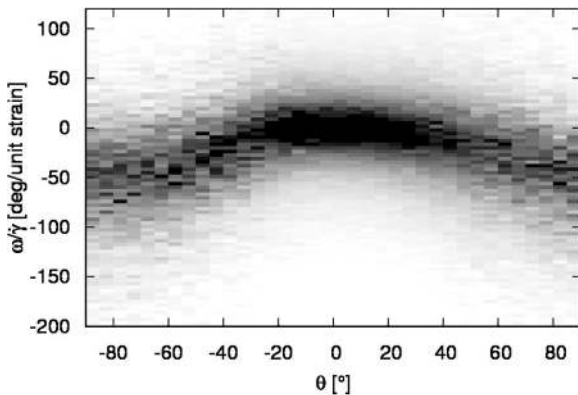

FIG. 8. Distribution of the rotation velocity ω of the particles as a function of their orientation θ in the stationary shear-aligned state for glass cylinders with $L/d = 3.5$. Data obtained by optical particle detection. In the grayscale plot black corresponds to the highest probability density.
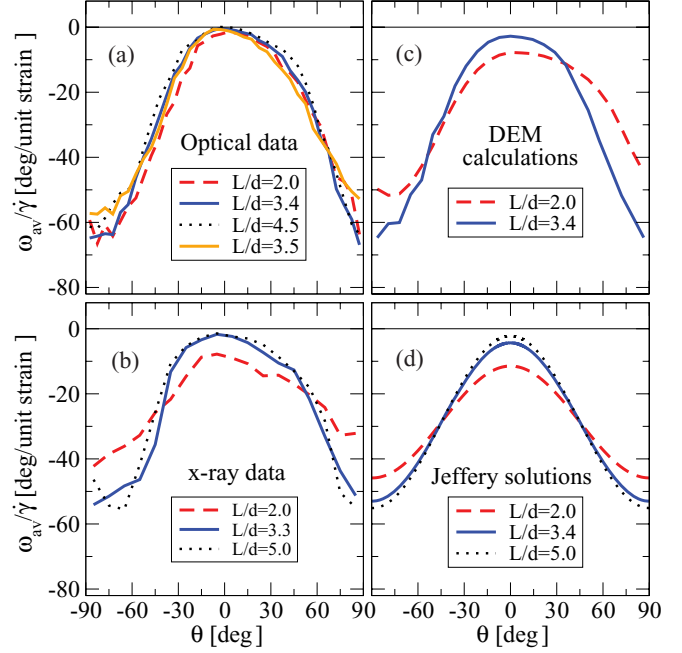

FIG. 9. (Color online) Normalized average rotation velocity of the particles $\omega_{av}/\dot{\gamma}$ as a function of their orientation θ for (a) rice and glass cylinders obtained by optical measurements (b) pegs obtained by x-ray tomography, (c) numerical simulations, and (d) hard ellipsoids in a sheared liquid as calculated by Jeffery [30].

materials, and plotted them against θ. Data from optical measurements are presented in Fig. 9(a) for rice grains with $L/d = 2.0, 3.4, 4.5$, and glass cylinders with 3.5, while Fig. 9(b) shows the results obtained by x-ray tomography for pegs with $L/d = 2.0, 3.3$ and 5.0. Figure 9(c) presents results obtained by numerical simulation (DEM). We have also included the result of the calculation by Jeffery [30], which describes the rotation velocity of a hard prolate ellipsoid immersed in a sheared viscous liquid. All four panels of Fig. 9 show similar tendencies, viz. the particles rotate faster when their orientation is far from the preferred one and rotate slower when they are closer to it. The ratio of these fast and slow rotation speeds appears to be smaller for shorter grains. In other words, longer grains show a stronger angular dependence of the rotation rates. Differences between our results for the granular particles and the Jeffery solutions arise from the grain-grain interactions.

B. Transients into the aligned steady state

So far, we have discussed the properties of the stationary state. In the following, we focus on the dynamics observed in the transient during which the system reaches the above described stationary state. Two types of experiments have been carried out: (a) starting from an initially random configuration, and (b) reversing the shear direction (i.e., starting from an oppositely shear-aligned state). The evolution of the distribution of particle angles has been investigated for glass cylinders with $L/d = 3.5$ taking (a) 1350 and (b) 1700 independent measurements, respectively. These measurements were performed using surface optical imaging, and the resulting probability
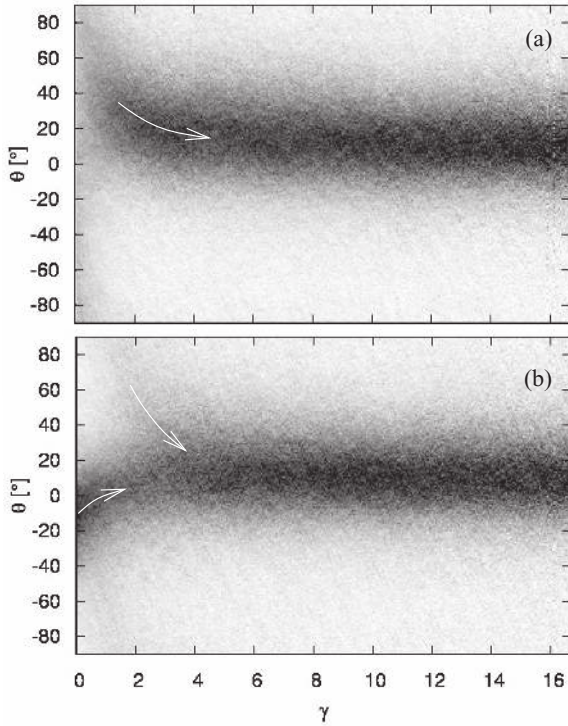
FIG. 10. Evolution of the orientational distribution of the particles (a) starting from an initially random orientation (b) from an aligned state after shear reversal. Both measurements were performed with glass cylinders with $L/d = 3.5$, data obtained by optical particle detection. In the grayscale plot, black corresponds to the highest probability density. The white arrow indicates the evolution of the center of the distribution for case (a). For case (b) the initially ordered state appears to split into two independently relaxing distributions, marked by white arrows.

distributions are plotted on Fig. 10 as a function of the strain (similarly to Fig. 7).

For the initially random system (a) we find a continuously increasing order and a decreasing alignment angle [see white arrow in Fig. 10(a)] both converging toward their stationary values. The evolution of the order parameter S and that of the average angle θ_{av} are shown as functions of γ in Figs. 11(a)–11(b). As it is seen, ordering develops faster than the convergence of the shear alignment angle. This can be quantified by the characteristic strain parameters of the approximately exponential relaxation, which are $\gamma_S = 0.73$ and $\gamma_\theta = 2.57$, respectively.

For initial condition (b) we find that the average angle rotates in the *opposite* direction, from $-\Theta_{av}$ to Θ_{av} [i.e., the majority of the grains turn backward and only a smaller fraction rotates forward as indicated by the two white arrows in Fig. 10(b)]. During this procedure the order parameter initially decreases then increases back to its stationary value as seen in Fig. 11(a). Interestingly the strain that is necessary to reach the stationary angle is about the same for the two initial conditions, but the strain needed to reach the stationary value of the order parameter is significantly different. To destroy and then recover the order takes about three times as much strain ($\gamma_S = 2.19$) compared to alignment from an initially random state ($\gamma_S = 0.73$).
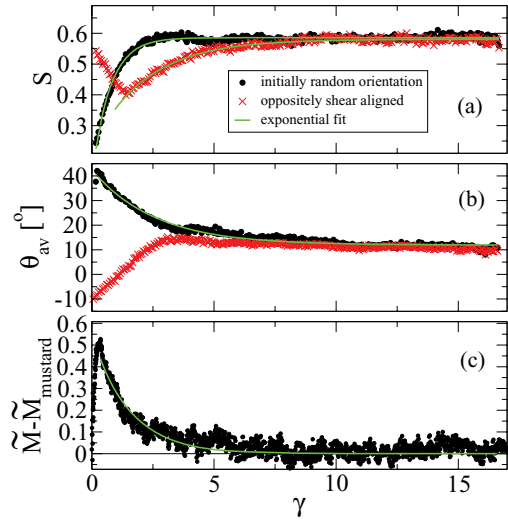

FIG. 11. (Color online) Evolution of the (a) order parameter and the (b) average alignment angle during both type of transients. Same measurement as in Fig. 10. (c) Evolution of the applied torque needed to maintain stationary rotation of the bottom plate starting from an initially random orientation. All measurements are for glass cylinders with $L/d = 3.5$. Continuous lines are fits assuming exponential relaxation, see text for the numerical values of the exponents.

It is very interesting to compare the normalized average particle rotation speed $\omega_{av}/\dot{\gamma}$ as a function of θ for these two different transients and the steady state [see Figs. 12(a)–12(b)]. In the stationary state, grains in all orientations θ rotate on average with negative ω (cf. Fig. 12, black circles). During the transients, we find a positive mean rotation velocity for grains between $-15°$ and $15°$. This means, that for both cases (a) and (b) these particles rotate against the direction dictated by the shear flow, while the rest of the particles rotate forward. Here, for the transients, the difference between cases (a) and (b) is that for the *oppositely shear aligned* transient the number of backward rotating grains is much larger due to the nature of the initial configuration. This is why the average reorientation
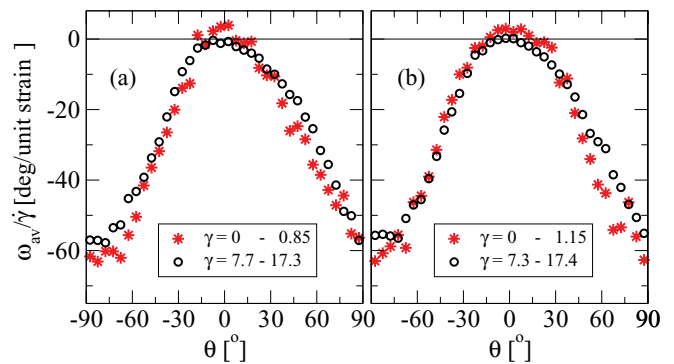

FIG. 12. (Color online) Normalized average rotation velocity of the particles $\omega_{av}/\dot{\gamma}$ as a function of their orientation θ during the two types of transients (a) starting from a random orientation (b) starting from a reversed flow-aligned state. Measurements done for glass cylinders with $L/d = 3.5$, data obtained by optical particle detection.

of the grains $\theta_{av}(\gamma)$ differs in the two cases [see white arrows indicating the grain rotation direction in Fig. 10 and the curves in 11(b)].

Additional measurements were performed for the initially random configuration (a). In these measurements we aimed to monitor the evolution of the effective friction of the sample during the transient. For this purpose we measured the torque M needed for a stationary rotation of the bottom plate, which was rescaled by the asymptotic value M_∞ as $\tilde{M} = M/M_\infty$. A reference data set was also recorded for nearly spherical mustard seeds, which is used to correct for effects not directly related to the reorientation of the sample. The rescaled and corrected curve is shown in Fig. 11(c). The first thing to note is that the ratio of the initial and final values of $\tilde{M}$ is around 1.5, suggesting that the effective friction of the unoriented sample is about 50% higher than that of the shear-aligned one. The second observation is that the evolution of the effective friction of the material can be described by an exponential decay of the excess torque as $\tilde{M} - \tilde{M}_{mustard} \approx (\tilde{M}_{max} - 1)e^{-\gamma/\gamma_M}$. This exponential fit results $\gamma_M = 1.46$, which is in between the characteristic values obtained for γ_S and γ_θ. Although the experimental curve is fairly noisy, one can pursue a more detailed analysis by fitting the data with the sum of two exponentials with decay rates of γ_S and γ_θ. The resulting amplitudes suggest that the evolution of S has a stronger influence on the evolution of M compared to the contribution of θ_{av}.

V. CONCLUSION

The orientation and rotation of elongated granular particles has been tracked in shear flow. In the asymptotic state, the time- and ensemble-averaged orientation of the particles forms a small angle Θ_{av} with the streamlines. This shear alignment angle is independent of shear rate and decreases with increasing particle aspect ratio. The characteristics of the

asymptotic alignment determined from optical experiments in this study are in good agreement with experiments obtained from x-ray computed tomography [27] of cylindrical pegs.

The average rotation speed of individual particles as a function of the orientation $\omega_{av}(\theta)$ shows that particles rotate faster if their orientation is perpendicular to the preferred average orientation and their rotation is slower when their orientation is near Θ_{av}. The ratio of this fast/slow rotation increases with grain aspect ratio, similarly to the case of a rotating hard ellipsoid in a sheared liquid as calculated by Jeffery [30]. In the stationary shear-aligned state the net rotation rate of particles is always negative (i.e., the sense of rotation is dictated by the shear flow). Transients into the asymptotic alignment have been studied starting from an (a) initially random configuration and (b) an oppositely shear-aligned state. The character of the transients depends upon the initial order and alignment. The transient is longer for case (b) where initial order is partially destroyed and then recovered again. A common feature of the two transients is that the particles with orientation just beyond Θ_{av} rotate backwards, and reach the preferred angle on a shorter way.

The evolution of the mechanical resistance of the sample measured during the transient indicates a 30% reduction of the materials effective friction during the course of the shear-induced ordering process.

[1] H. M. Jaeger, S. R. Nagel, and R. P. Behringer, Rev. Mod. Phys. **68**, 1259 (1996).

[2] I. S. Aranson and L. S. Tsimring, Rev. Mod. Phys. **78**, 641 (2006).

[3] P. Jop, Y. Forterre, and O. Pouliquen, Nature (London) **441**, 727 (2006).

[4] GDR MiDi, Eur. Phys. J. E **14**, 341 (2004).

[5] V. Kumaran and S. Maheshwari, Phys. Fluids **24**, 053302 (2012).

[6] R. P. Behringer and G. W. Baxter, in *Granular Matter, An interdisciplinary approach*, edited by A. Mehta (Springer, New York, 1994), p. 85.

[7] H. Ehrentraut and A. Chrzanowska, in *Dynamic response of granular and porous materials under large and catastrophic deformations*, edited by K. Hutter and N. P. Kirchner (Springer, Berlin, 2003), p. 343.

[8] A. A. Peña, R. García-Rojo, and H. J. Hermann, Granular Matter **9**, 279 (2007).

[9] C. S. Campbell, Phys. Fluids **23**, 013306 (2011).

[10] W. Losert, L. Bocquet, T. C. Lubensky, and J. P. Gollub, Phys. Rev. Lett. **85**, 1428 (2000).

[11] F. da Cruz, S. Emam, M. Prochnow, J-N. Roux, and F. Chevoir, Phys. Rev. E **72**, 021309 (2005).

[12] L. E. Silbert, D. Ertas, G. S. Grest, T. C. Halsey, D. Levine, and S. J. Plimpton, Phys. Rev. E **64**, 051302 (2001).

[13] N. Taberlet, P. Richard, J. T. Jenkins, and R. Delannay, Eur. Phys. J. E **22**, 17 (2007).

[14] J.-F. Métayer, D. J. Suntrup, C. Radin, H. L. Swinney, and M. Schröter, Europhys. Lett. **93**, 64003 (2011).

[15] T. Börzsönyi, T. C. Halsey, and R. E. Ecke, Phys. Rev. Lett. **94**, 208001 (2005).

[16] T. Börzsönyi and R. E. Ecke, Phys. Rev. E **74**, 061301 (2006).

[17] T. Börzsönyi and R. E. Ecke, Phys. Rev. E **76**, 031301 (2007).

[18] T. Börzsönyi, R. E. Ecke, and J. N. McElwaine, Phys. Rev. Lett. **103**, 178302 (2009).

[19] E. Azéma and F. Radjaï, Phys. Rev. E **81**, 051304 (2010).

[20] E. Azéma and F. Radjaï, Phys. Rev. E **85**, 031303 (2012).

[21] D. Fenistein and M. van Hecke, Nature (London) **425**, 256 (2003).

[22] D. Fenistein, J. W. van de Meent, and M. van Hecke, Phys. Rev. Lett. **92**, 094301 (2004).

[23] S. Luding, Particuology **6**, 501 (2008).

[24] L. Brendel, J. Török, R. Kirsch, and U. Bröckel, Granular Matter **13**, 777 (2012).

[25] T. Börzsönyi, B. Szabó, G. Törös, S. Wegner, J. Török, E. Somfai, T. Bien, and R. Stannarius, Phys. Rev. Lett. **108**, 228302 (2012).

[26] J. A. Dijksman, E. Wandersman, S. Slotterback, C. R. Berardi, W. D. Updegraff, M. van Hecke, and W. Losert, Phys. Rev. E **82**, 060301 (2010).

[27] S. Wegner, T. Börzsönyi, T. Bien, G. Rose, and R. Stannarius, Soft Matter **8**, 10950 (2012).

[28] S. Plimpton, J. Comput. Phys. **117**, 1 (1995).

[29] Z. Shojaaee, L. Brendel, J. Török, and D. E. Wolf, Phys. Rev. E **86**, 011302 (2012).

[30] G. B. Jeffery, Proc. R. Soc. London A **102**, 161 (1922).